[redacted]

NASA TM SX-685

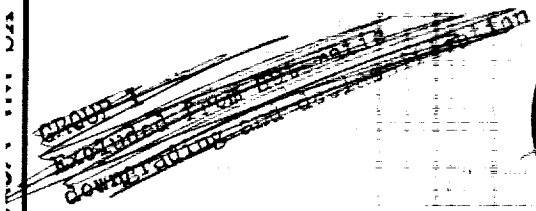

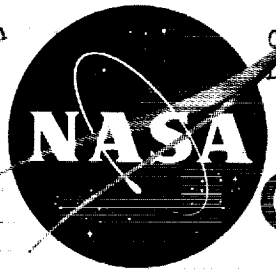

TECHNICAL MEMORANDUM

SX-685

for the

U.S. Air Force

JET INTERFERENCE EFFECTS ON A MODEL OF A SINGLE-ENGINE FOUR-JET V/STOL AIRPLANE AT MACH NUMBERS FROM 0.60 TO 1.00

By James W. Schmeer and Jack F. Runckel

Langley Research Center
Langley Air Force Base, Va.

SERVICE REPORT

[redacted]

NATIONAL AERONAUTICS AND SPACE ADMINISTRATION

WASHINGTON

MAR 16 1962

[redacted]

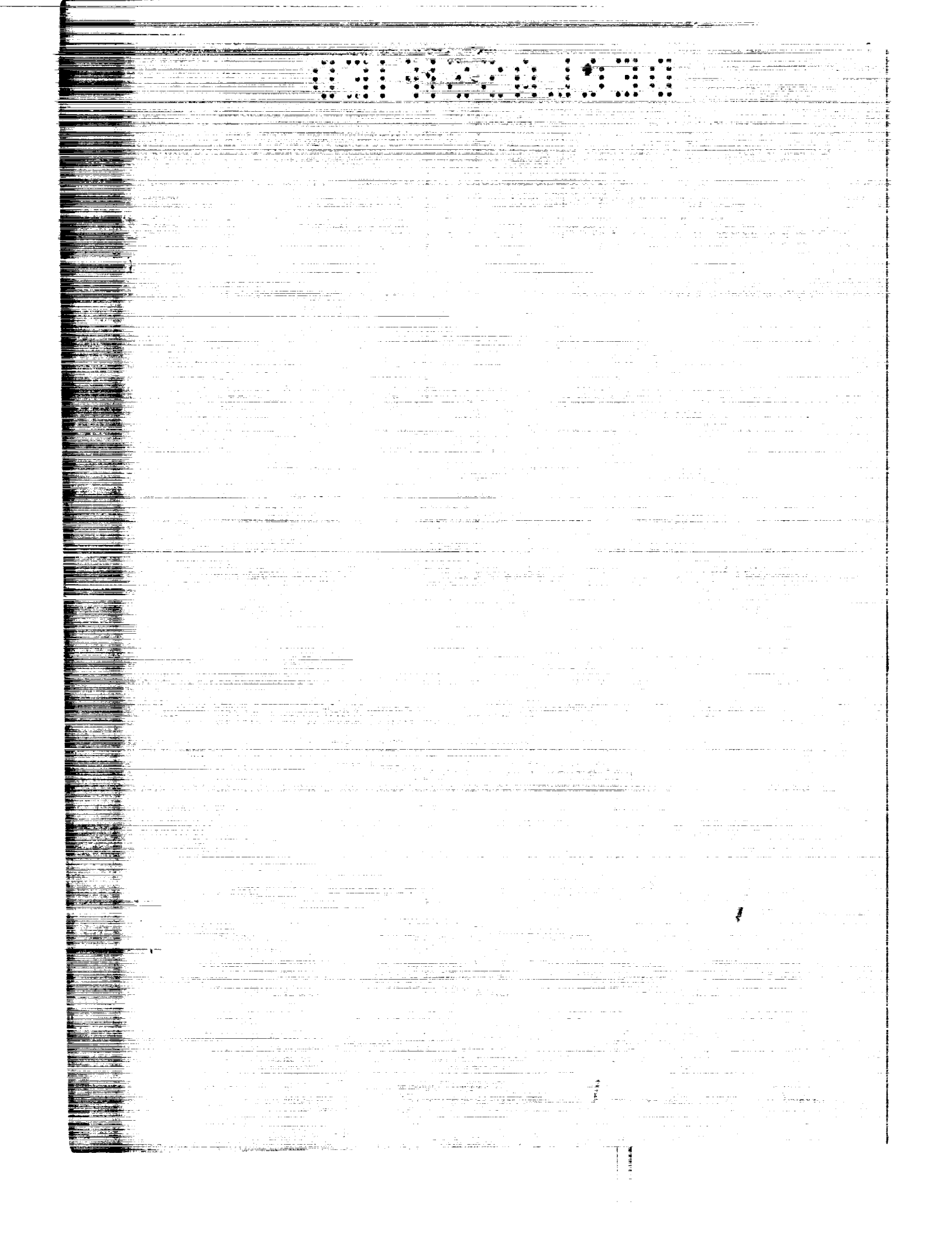

NATIONAL AERONAUTICS AND SPACE ADMINISTRATION

TECHNICAL MEMORANDUM SX-685

for the

U.S. Air Force

JET INTERFERENCE EFFECTS ON A MODEL OF A SINGLE-ENGINE FOUR-JET V/STOL AIRPLANE AT MACH NUMBERS FROM 0.60 TO 1.00*

By James W. Schmeer and Jack F. Runckel

SUMMARY

An investigation was conducted in the Langley 16-foot transonic tunnel to determine the interference from four exhaust jets on the aerodynamic characteristics of a model of a V/STOL airplane. The single-engine four-jet turbofan power plant of the airplane was simulated by inducing tunnel airflow through two large side inlets and injecting the decomposition products of hydrogen peroxide into the internal flow. The heated gas mixture was exhausted through four nozzles located on the sides of the fuselage under the wing, two near the wing leading edge and two forward of the trailing edge; the nozzles were deflected downward 1.5° and outward 5.0° to simulate cruise conditions. The wing of the model was a clipped delta with leading-edge sweep of 40°, aspect ratio of 3.06, taper ratio of 0.218, thickness-chord ratio of 0.09 at the root and 0.07 at the tip, and 10° negative dihedral. Aerodynamic and longitudinal stability coefficients were obtained for the model with the tail removed, and for horizontal-tail incidences of 0° and -5°. Data were obtained at Mach numbers from 0.60 to 1.00, angles of attack from 0° to 12°, and with jet total-pressure ratios up to 3.1.

Jet operation generally caused a decrease in lift, an increase in pitching-moment coefficient, and a decrease in longitudinal stability at subsonic speeds. The jet interference effects on drag were detrimental at a Mach number of 0.60 and favorable at higher speeds for cruising-flight attitudes.

---

* Title, Unclassified.

INTRODUCTION

One of the promising airplane configurations, which has been proposed for fighter-strike missions, utilizes a single turbofan engine and four swiveling exhaust nozzles in order to achieve vertical, or short, take-offs and landings as well as a high subsonic cruising capability. Available in reference 1 are the results of an investigation of the dynamic stability and control characteristics of a jet-powered model of the airplane in hovering and transition flight. Results of a power-off investigation of the transonic performance and stability characteristics of a 1/8-scale model of this airplane conducted in the Langley 16-foot transonic tunnel are presented in reference 2. Because the location of the exhaust nozzles along the fuselage and close to the wing could lead to significant jet interference effects on the aerodynamic characteristics, a power-on investigation, utilizing the same model and facility, was undertaken to determine these effects and the results are presented herein.

In the present tests, free-stream air was inducted through two large side inlets, mixed with the decomposition products of 90-percent hydrogen peroxide (see ref. 3), and the resulting heated gas mixture exhausted through the exit nozzles. The nozzles, which were located on each side of the fuselage just under the wing, were canted downward 1.5° and outward 5.0° to simulate cruise conditions.

The effects of jet interference on lift, drag, and pitching-moment characteristics were investigated for the model with tail removed and for the model with horizontal-tail incidences of 0° and -5°. Data were obtained at Mach numbers from 0.60 to 1.00, angles of attack from 0° to 12°, and jet total-pressure ratios up to 3.1.

SYMBOLS

$A_1, A_2, \ldots, A_7$ model areas (fig. 4)

C_D drag coefficient, $\frac{\text{Drag}}{qS}$

C_L lift coefficient, $\frac{\text{Lift}}{qS}$

C_m pitching-moment coefficient, $\frac{\text{Pitching moment}}{qS\bar{c}}$

$\bar{c}$	mean aerodynamic chord
i_t	horizontal-tail incidence, positive for leading edge rotated upward
F_{MB}	main-balance axial force, measured (positive in same sense as drag)
F_{MB}'	main-balance axial force, corrected (fig. 4)
M	free-stream Mach number
p	free-stream static pressure
p_b	base pressure
p_i	internal pressure
$p_{t,j}$	jet total pressure (average of rear exits)
q	free-stream dynamic pressure
S	wing area (plan-view projection)
α	angle of attack referenced to fuselage center line
ΔC_D	jet-induced incremental drag coefficient
ΔC_L	jet-induced incremental lift coefficient
ΔC_m	jet-induced incremental pitching-moment coefficient
θ_1, θ_2	engine-nozzle-shroud cut-off angles (fig. 4)

APPARATUS AND METHODS

The investigation was conducted in the Langley 16-foot transonic tunnel, which is an atmospheric wind tunnel with a slotted test section.

Model

External arrangement.- A sketch of the 1/8-scale model of a V/STOL airplane, with a table of significant dimensions, is shown in figure 1.

[redacted]

Photographs of the model installed in the Langley 16-foot transonic tunnel are shown in figure 2. In order to accommodate the supporting sting, the rearward 11 percent of the fuselage was enlarged and, therefore, was not geometrically similar to that of the airplane.

The wing had a symmetrical airfoil section at the root. The airfoil section at the wing tip had an effective camber of 3.6 percent of the local chord as a result of curvature of the forward 30 percent of the mean line, and had a symmetrical thickness distribution over the rearward 70 percent. The maximum thickness of the wing was located at 37.5 percent of the local chord. The thickness and camber of the intermediate airfoil sections varied linearly along the wing semispan from the values at the root to those at the tip.

The model had two large side inlets with rounded lips. Diverter plates extending forward from the inlets along the fuselage separated the boundary-layer air from the inlet flow.

Propulsion system.- A photograph of the hydrogen-peroxide gas generator and internal ducting system is presented in figure 3. Liquid hydrogen peroxide was piped into a single cylindrical decomposition chamber located between the duct inlets. From a settling chamber directly aft of the decomposition chamber, the gas products were divided equally between the left and right ducts where they were ejected rearward through 24 small supersonic ejector nozzles (per duct). Six ejector nozzles were spaced across the downstream end of each of four struts in each duct located just aft of the inlet. (See fig. 2(a).) The resulting mixture of hot gas products and inlet air was again divided between the front and rear exits. In this investigation, the four engine exhaust nozzles were canted downward 1.5° and outward 5.0° to simulate cruise conditions.

Instrumentation

Force balances.- Shown in figure 4 is a schematic diagram of the balance, duct, and seal arrangement. The two ducts, indicated by hatching, were attached to a six-component strain-gage balance which sensed all the internal forces except those exerted on a short portion of the inlets forward of the flexible seals. The main six-component strain-gage balance sensed forces acting on the entire model, including internal forces.

Pressure instrumentation.- Pressures were measured at several locations in that part of the model interior which forms a common chamber forward of the rear flexible seal and external to the ducts (p_i) and in the base cavity behind the rear seal (p_b). (See fig. 4.) Total pressures

in each duct were measured ahead of the turning vanes in the rear set of nozzles. Rakes were installed in the inlets during special tests to determine the mass-flow ratios. All pressures were obtained from strain-gage pressure transducers and recorded in punch cards along with the force data.

Tests

The model had boundary-layer transition fixed on the wing and tail surfaces by means of 1/8-inch-wide bands of No. 180 carborundum grains located at 2.5 percent of the local chord. Similar transition strips were located around the nose of the fuselage at 2.5 percent of the body length and on the external surfaces of the inlets just aft of the inlet lips.

Power-off and power-on force and moment data were obtained at Mach numbers of 0.60, 0.80, 0.90, and 1.00 at angles of attack of 0°, 4°, 8°, and 12°. The model was tested with the tail at $i_t = 0^\circ$ and -5° and with the horizontal tail removed. The average Reynolds number per foot was approximately 3.8×10^6.

Free-stream air was inducted through the inlets and exhausted through the exits for all tests. For the power-on tests, the decomposition products of hydrogen peroxide were ejected into the ducts and mixed with the inlet air. Jet total-pressure ratio was varied by adjusting the hydrogen peroxide mass-flow rate. Jet total temperatures also varied with mass-flow rate as well as with Mach number and free-stream stagnation temperature; the values ranged from about 300° F at the lowest values of $p_{t,j}/p$ to 950° F at the highest values.

The introduction of mass flow within the ducts during jet operation caused a reduction in the inlet mass flow which affected the inlet lip forces. Therefore, jet-off tests were made with several different size plugs in the exits in order to vary inlet mass flow and thus permit evaluation of the effects on inlet forces; the results could then be applied as tare corrections to the jet-on data.

Data Reduction

The axial force measured by the main balance was adjusted to a condition of free-stream static pressure both at the fuselage base and in the fuselage cavity. (See fig. 4.) Note that the corrections to axial force due to pressure acting on the annular area around the nozzle is applied because these annular areas do not exist on the actual airplane. The net external forces and moments were obtained by subtracting

[redacted]

those measured by the duct balance from those measured by the main balance, after transfer to model moment center. Then, in order to obtain the jet-induced or incremental aerodynamic characteristics, the net external forces and moments for the power-off test points were subtracted from the corresponding power-on results. Finally, corrections to the data were made to account for the variation of inlet lip forces caused by a reduction in inlet mass flow during jet operation. These corrections, or tares, which were obtained in separate tests described in the previous section, were applied for the condition of equal inlet mass-flow ratios for the exit plug tests and the power-on tests. This, in effect, adjusted the power-on data to a condition of constant inlet mass flow (jet-off values shown in ref. 2) for a given Mach number and angle of attack, regardless of the jet total-pressure ratio.

RESULTS AND DISCUSSION

Because of the complicated interactions possible between the jet exhausts and the wing, fuselage, and tail surfaces, and the model flow field, a detailed analysis of the interference effects without the benefit of extensive pressure instrumentation is not feasible. The discussion of the results, therefore, will be confined to relating overall trends and relative magnitudes.

The basic data in the form of jet-induced incremental coefficients are plotted against jet total-pressure ratio in figures 5, 6, and 7 for the model with the horizontal tail removed, for $i_t = 0^\circ$, and for $i_t = -5^\circ$, respectively. With the assumed schedule of jet total-pressure ratio with Mach number shown in figure 8, the incremental coefficients for these tail configurations are replotted with angle of attack as a variable in figure 9. The variation of model angle of attack, drag coefficient, and pitching-moment coefficient with lift coefficient is presented for scheduled pressure ratios with the jets operating in figure 10 and compared with data for the jets off.

Jet-Induced Incremental Coefficients

Lift.- For the model with the horizontal tail removed, figure 5(a) shows that operation of the jets caused a slight loss in lift at Mach numbers up to 0.90, except at $\alpha = 12^\circ$ for $M = 0.80$ and 0.90. Lift increased with increasing total-pressure ratio at $M = 1.00$. Figures 6(a) and 7(a) show similar trends and magnitudes of ΔC_L for the model with $i_t = 0^\circ$ and $i_t = -5^\circ$, respectively. The similarity of the jet effects on lift for the three configurations is further

illustrated in figure 9; here it is noted at subsonic speeds that at constant pressure ratio, ΔC_L generally becomes more positive with increasing angle of attack. The small effect due to the tail indicates that the change in lift due to jet operation must occur primarily on the wing, probably because of the close proximity of the jet exits to the undersurface of the wing.

Drag.- The incremental drag coefficients for the model without a horizontal tail, presented in figure 5(b), show that the drag increases slightly with jet total-pressure ratio above the exit choke point (pressure ratios > 1.8) at a Mach number of 0.60. At Mach numbers of 0.80 and 0.90, which are in the initial portion of the drag rise (see ref. 2), the jet effects are variable and tend to become favorable with increasing total-pressure ratio for the lower angles of attack; however, these effects tend to become unfavorable at the higher angles, particularly at 12° for a Mach number of 0.90. With an increase of speed to $M = 1.00$, drag increases with jet total-pressure ratio at all angles of attack. Data for the horizontal tail added at zero incidence (fig. 6(b)) show trends with jet total-pressure ratio, angle of attack, and Mach number similar to those with the horizontal tail removed. However, in the drag-rise region ($M = 0.80$ and $M = 0.90$) the favorable interference effects are usually greater, which may be attributable to a flow-field change at the rear of the model due to the addition of the horizontal-tail surfaces. The more favorable jet effects due to the tail is apparent throughout the angle-of-attack range for these speeds in figure 9. Again, although there are some changes in level, the trends are similar for the model with $i_t = -5^\circ$. (See figs. 7(b) and 9.) The generally favorable jet interference effects are similar to those that have been obtained from pressure measurements on airplane configuration afterbodies (refs. 4 and 5), and with force measurements on the fuselage-tail portion of an airplane model (ref. 6).

Pitching moment.- Increasing jet total-pressure ratio tended to increase the tail-off incremental pitching-moment coefficients at subsonic speeds up to angles of attack of 8° (fig. 5(c)). At an angle of attack of 12° and Mach numbers of 0.80 and 0.90 and at all angles of attack at a Mach number of 1.00, the incremental pitching-moment coefficients generally decreased as the jet total-pressure ratio increased. With the horizontal tail at $i_t = 0^\circ$ and -5° (figs. 6(c) and 7(c)), the trends were similar except in the drag-rise speed range at the highest angles of attack, where the incremental pitching-moment coefficients increased with increasing pressure ratio. These results are similar to the positive fuselage-tail incremental pitching-moment coefficients obtained with other jet-powered configurations having relatively low horizontal tails. (See refs. 5 and 6.) The differences in the variation of incremental pitching-moment coefficient with angle of attack for the three different tail configurations (fig. 9) illustrate the

influence of the jet exhaust on the tail surfaces. At subsonic speeds, there appears to be some opposing trends between the tail-on and the tail-off data but at $M = 1.00$, the effects are similar.

Aerodynamic Characteristics for Model With and Without Jet Operation

Comparisons of the aerodynamic characteristics for the model ($i_t = 0^\circ$) with and without jet operation, presented in figure 10, indicate that at cruising-flight attitudes (ref. 2), simulated jet operation decreased lift and made the pitching-moment coefficients more positive at subsonic speeds. Drag coefficients at constant lift coefficient increased slightly at $M = 0.60$ and decreased at higher subsonic Mach numbers. At a Mach number of 1.00 the effects of jet operation on lift and pitching-moment coefficients were the opposite of those at subsonic speeds. Slight decreases in longitudinal stability due to jet operation occurred at subsonic speeds with opposite effects at a Mach number of 1.00.

SUMMARY OF RESULTS

The results of an investigation to determine the jet interference effects on a model of a single-engine four-jet V/STOL airplane at cruise conditions may be summarized as follows:

1. Jet operation caused the lift to decrease at subsonic speeds for angles of attack below 12°.

2. The jet interference effects on drag varied with Mach number and angle of attack; the effects were generally detrimental at a Mach number of 0.60 and favorable at higher speeds for cruising-flight attitudes.

3. Jet operation produced an increase in pitching-moment coefficient and a decrease in longitudinal stability at subsonic speeds with opposite effects at a Mach number of 1.00.

Langley Research Center,
National Aeronautics and Space Administration,
Langley Air Force Base, Va., March 1, 1962.

REFERENCES

1. Smith, Charles C., Jr.: Flight Tests of a 1/6-Scale Model of the Hawker P 1127 Jet VTOL Airplane. NASA TM SX-531, 1961.

2. Schmeer, James W., Cassetti, Marlowe D., and Simonson, Albert J.: Transonic Aerodynamic Characteristics of a Model of a Single-Engine Four-Jet V/STOL Airplane. NASA TM SX-528, 1961.

3. Runckel, Jack F., and Swihart, John M.: A Hydrogen Peroxide Hot-Jet Simulator for Wind-Tunnel Tests of Turbojet-Exit Models. NASA MEMO 1-10-59L, 1959.

4. Lee, Edwin E., Jr., and Salters, Leland B., Jr.: Effects of Afterbody Shape and Hot Jet Exhausts on Pressure, Temperatures, and Drag of a Twin-Engine Fighter-Airplane Model Having an Overhanging Fuselage. NASA MEMO 12-29-58L, 1959.

5. Lee, Edwin E., Jr., Foss, Willard E., Jr., and Runckel, Jack F.: Jet Effects on the Base, Afterbody, and Tail Regions of a Twin-Engine Airplane Model With High and Low Horizontal-Tail Locations. NASA TM X-2, 1959.

6. Lee, Edwin E., Jr., and Mercer, Charles E.: Jet Interference Effects on a Twin-Engine Attack-Type-Airplane Model With Large Speed-Brake, Thrust-Spoiler Surfaces. NASA TM X-454, 1961.

Wing	
Area, sq ft	2.93
Aspect ratio	3.06
Taper ratio	0.218
Leading-edge sweep, deg	40
Span, in.	35.94
Root chord, in.	19.25
Tip chord, in.	4.21
Mean aerodynamic chord, in.	13.52
Root thickness, percent chord	9
Tip thickness, percent chord	7
Incidence, deg	1
Horizontal tail	
Area, sq ft	0.572
Aspect ratio	2.73
Taper ratio	0.314
Leading-edge sweep, deg	45
Span, in.	15
Root chord, in.	8.37
Tip chord, in.	2.62
Root thickness, percent chord	7
Tip thickness, percent chord	7
Vertical tail	
Area, sq ft	0.401
Taper ratio	0.275
Leading-edge sweep	50°25'
Height, in.	7.56
Root chord, in.	11.13
Tip chord, in.	3.06
Root thickness, percent chord	8
Tip thickness, percent chord	7

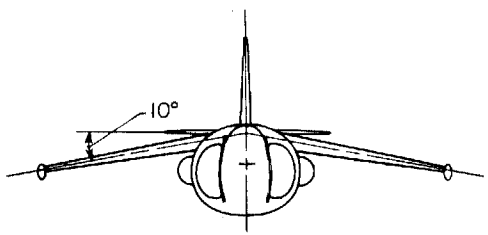

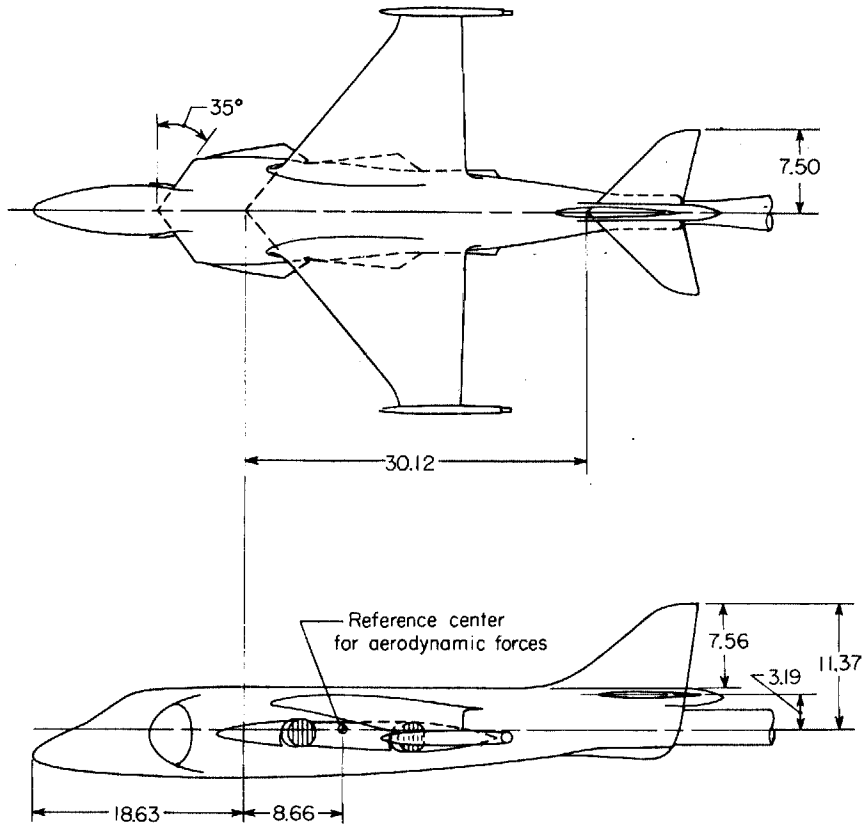

Figure 1.- Drawing of four-jet V/STOL model. All dimensions in inches.

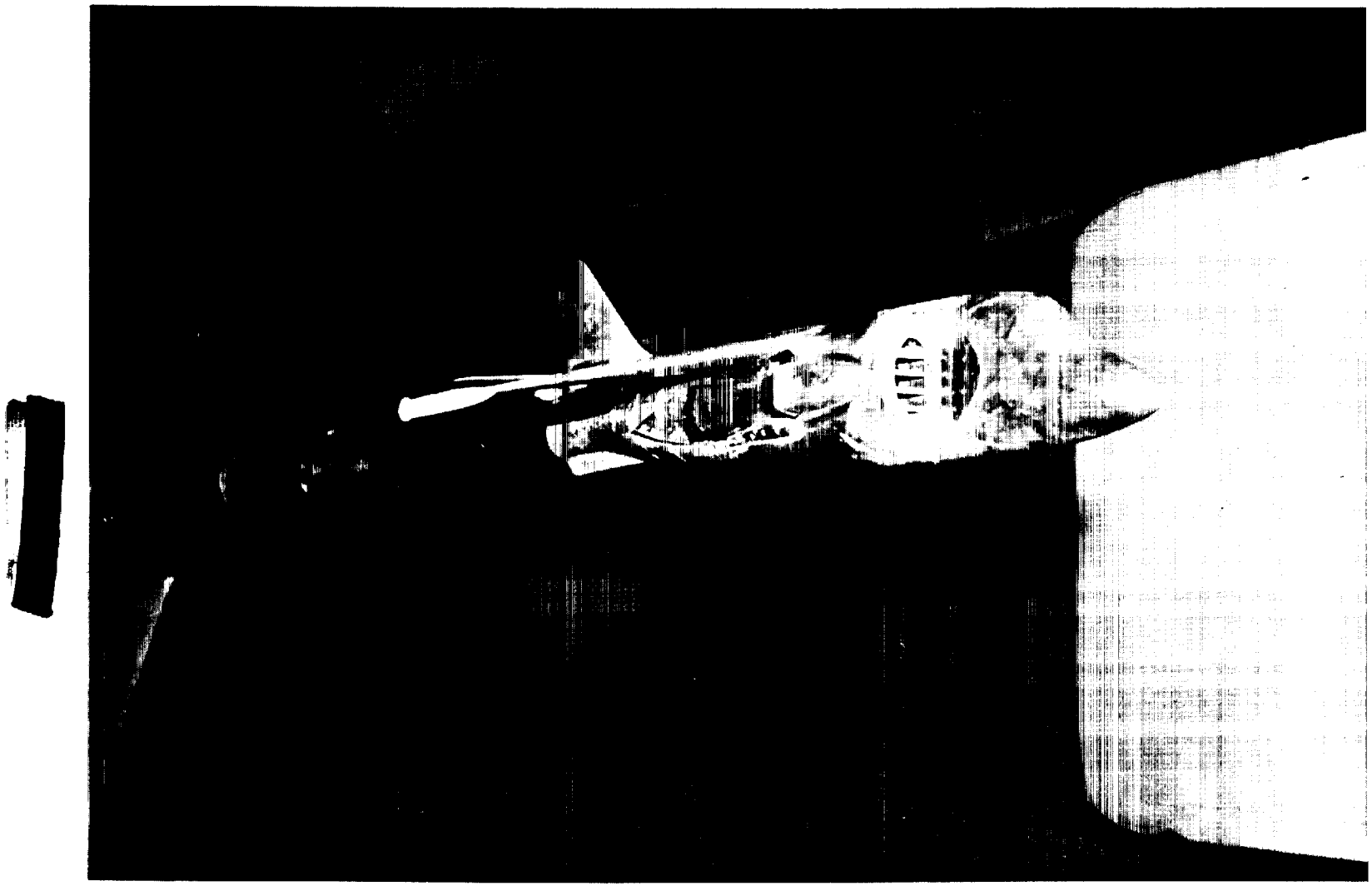

(a) Three-quarter front view. L-60-2170

Figure 2.- Photograph of four-jet V/STOL model mounted in the Langley 16-foot transonic tunnel.

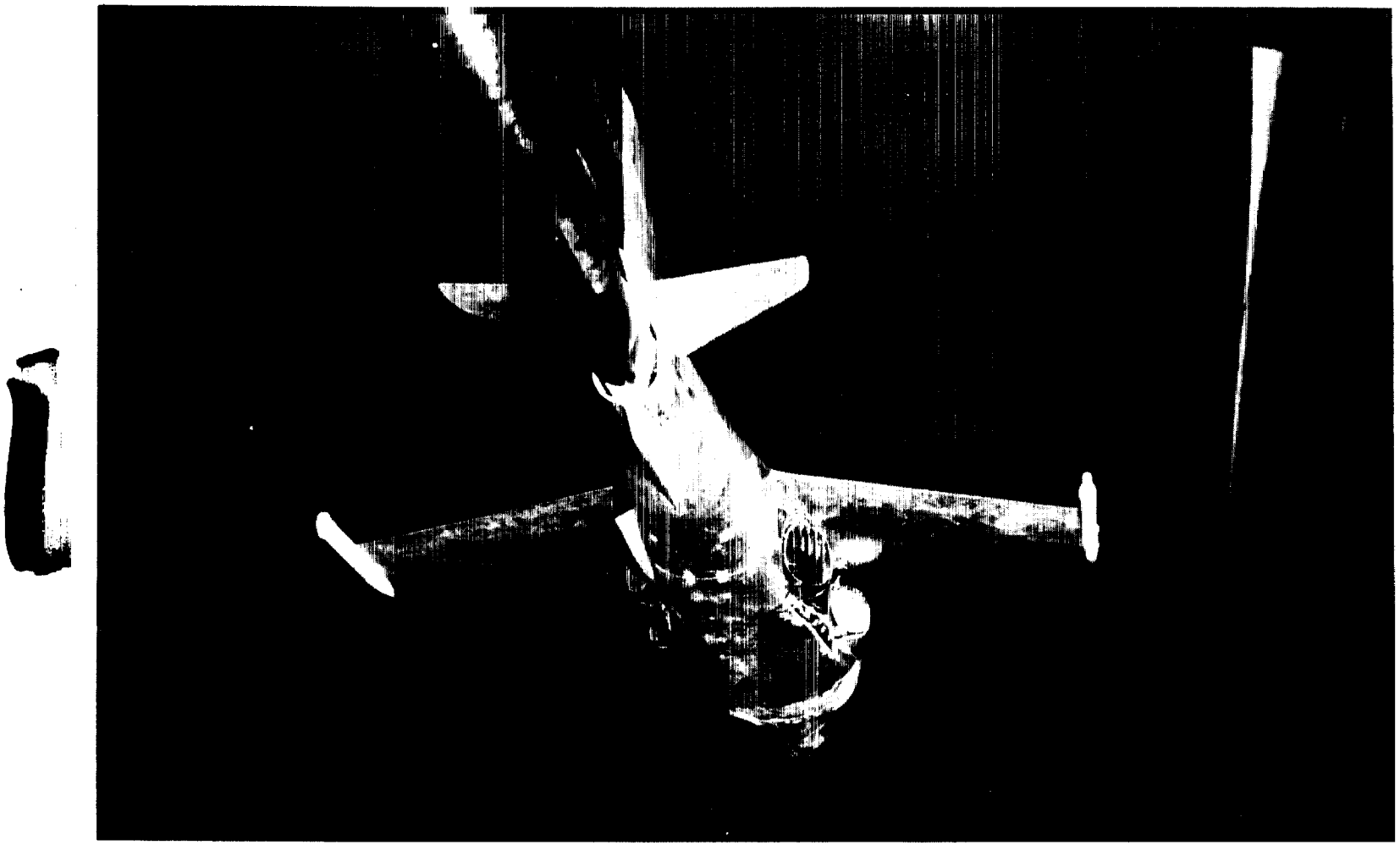

(b) Rear view. L-60-2171

Figure 2.- Concluded.

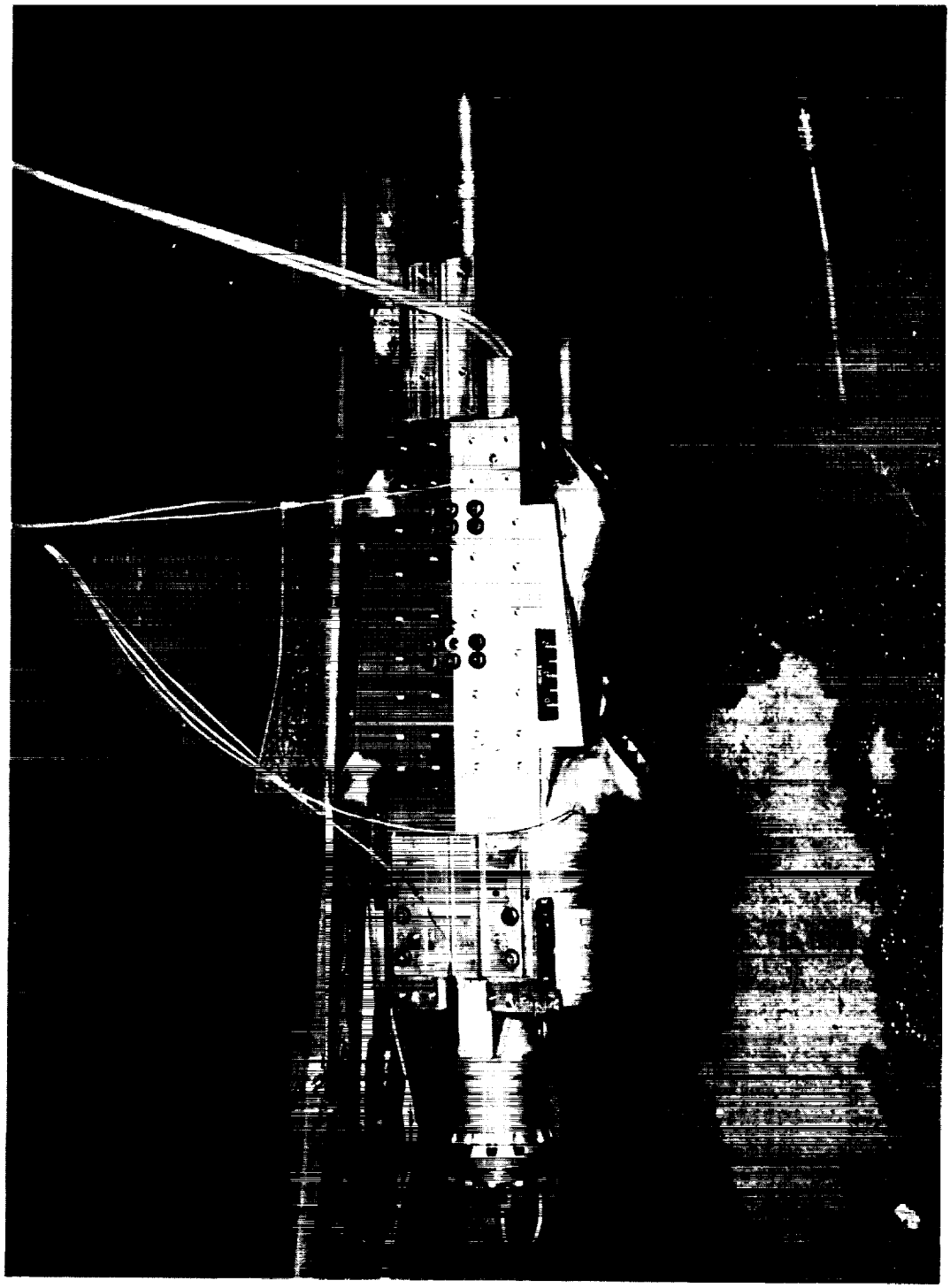

L-62-42

Figure 3.- Photograph of power plant.

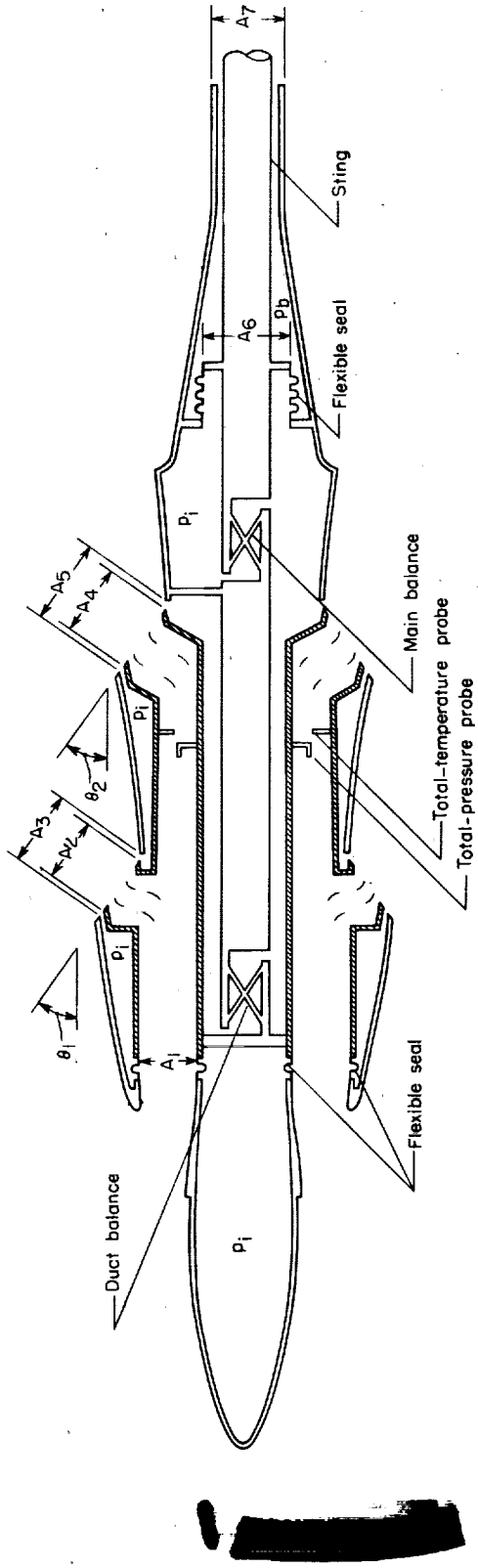

$$F_{MB}' = F_{MB} + 2(p_i - p)\left[(A_3 - A_2)\sin\theta_1 + (A_5 - A_4)\sin\theta_2\right] + (p_i - p_b)A_6 + (p_b - p)A_7$$

Figure 4.- Schematic diagram of balance, duct, and seal arrangement.

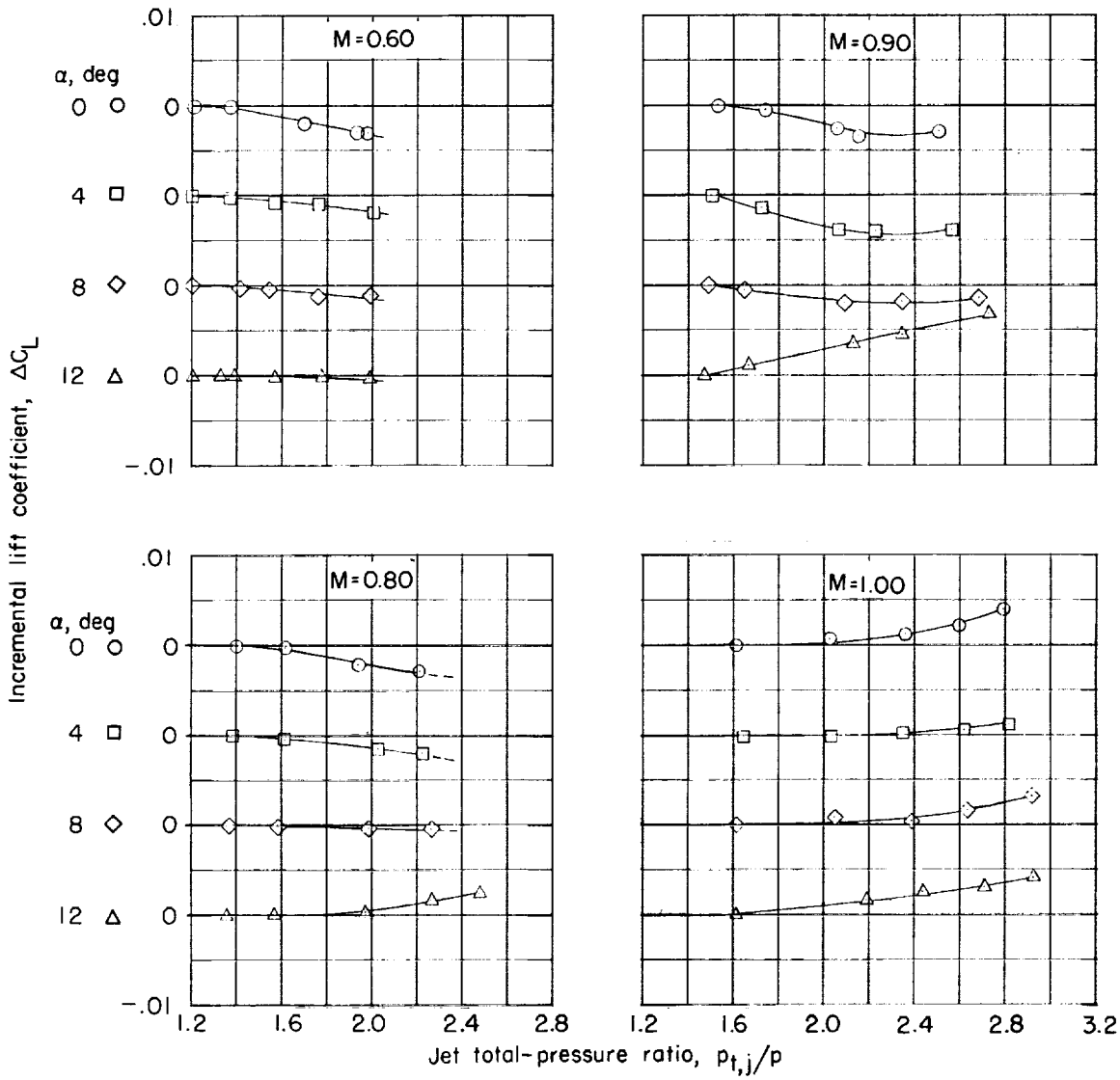

(a) Variation of incremental lift coefficient with jet total-pressure ratio.

Figure 5.- Jet effects on aerodynamic characteristics of model with horizontal tail off.

[redacted]

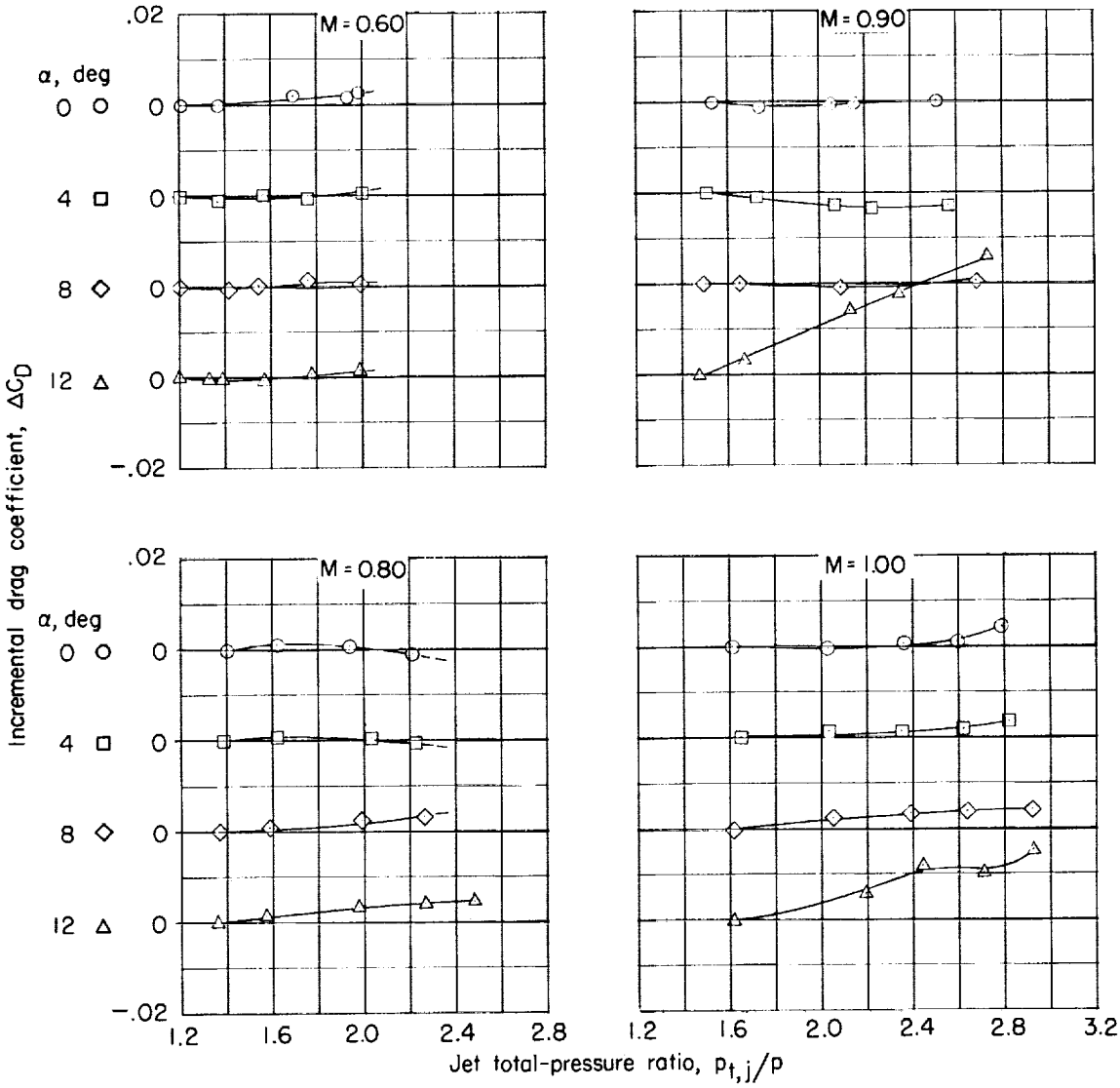

(b) Variation of incremental drag coefficient with jet total-pressure ratio.

Figure 5.- Continued.

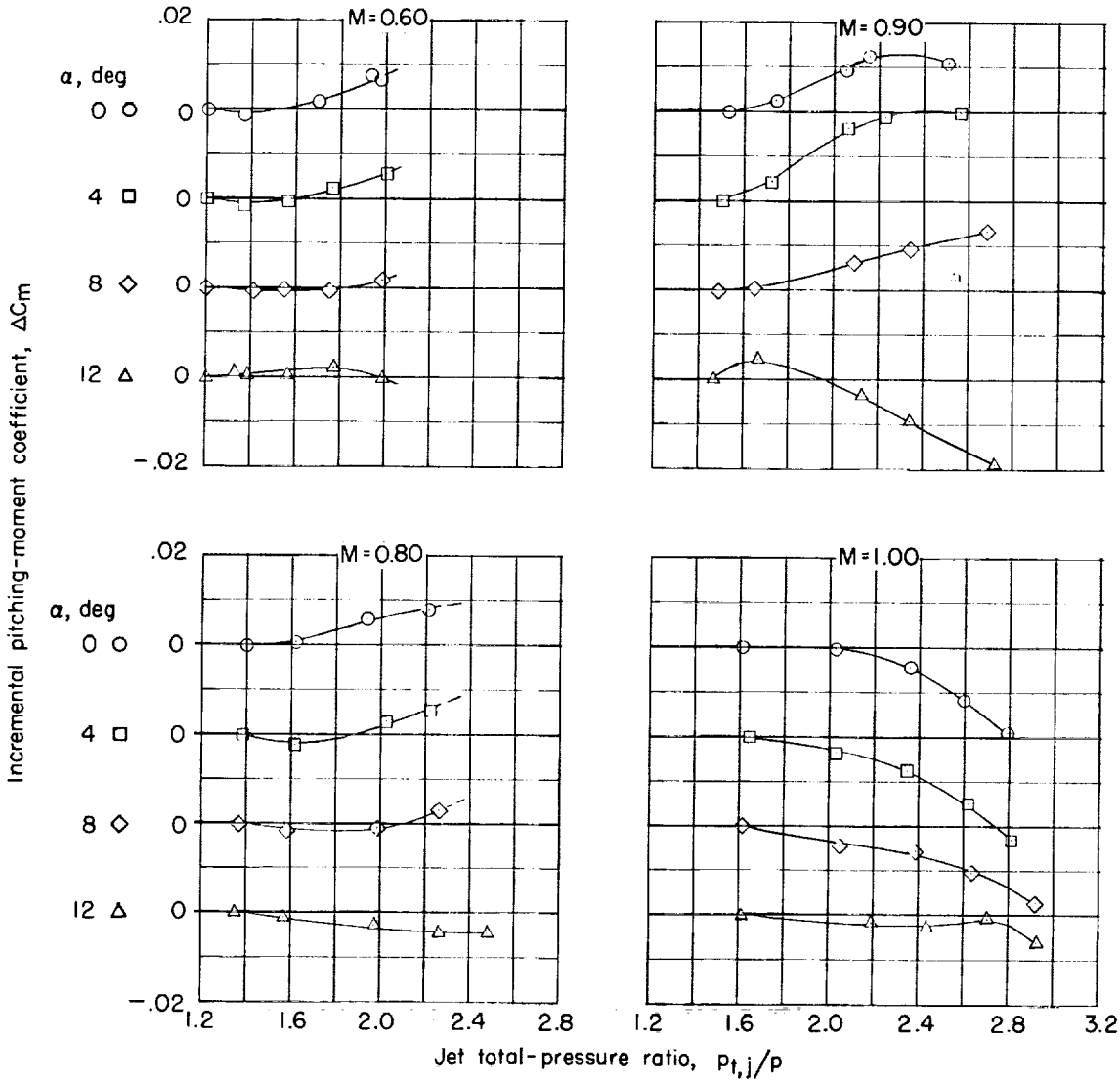

(c) Variation of incremental pitching-moment coefficient with jet total-pressure ratio.

Figure 5.- Concluded.

[redacted]

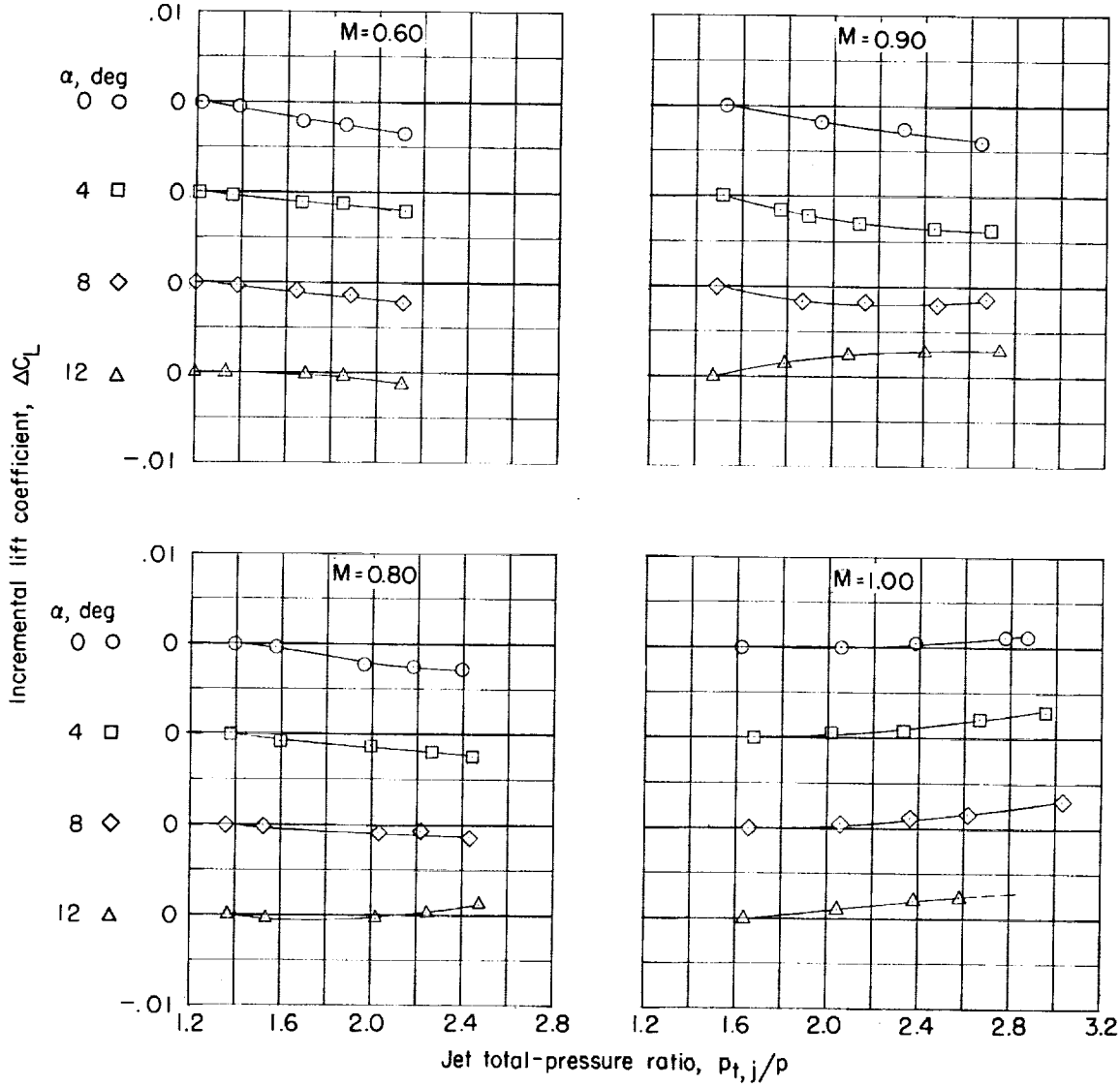

(a) Variation of incremental lift coefficient with jet total-pressure ratio.

Figure 6.- Jet effects on aerodynamic characteristics of model with horizontal-tail incidence set at $i_t = 0^\circ$.

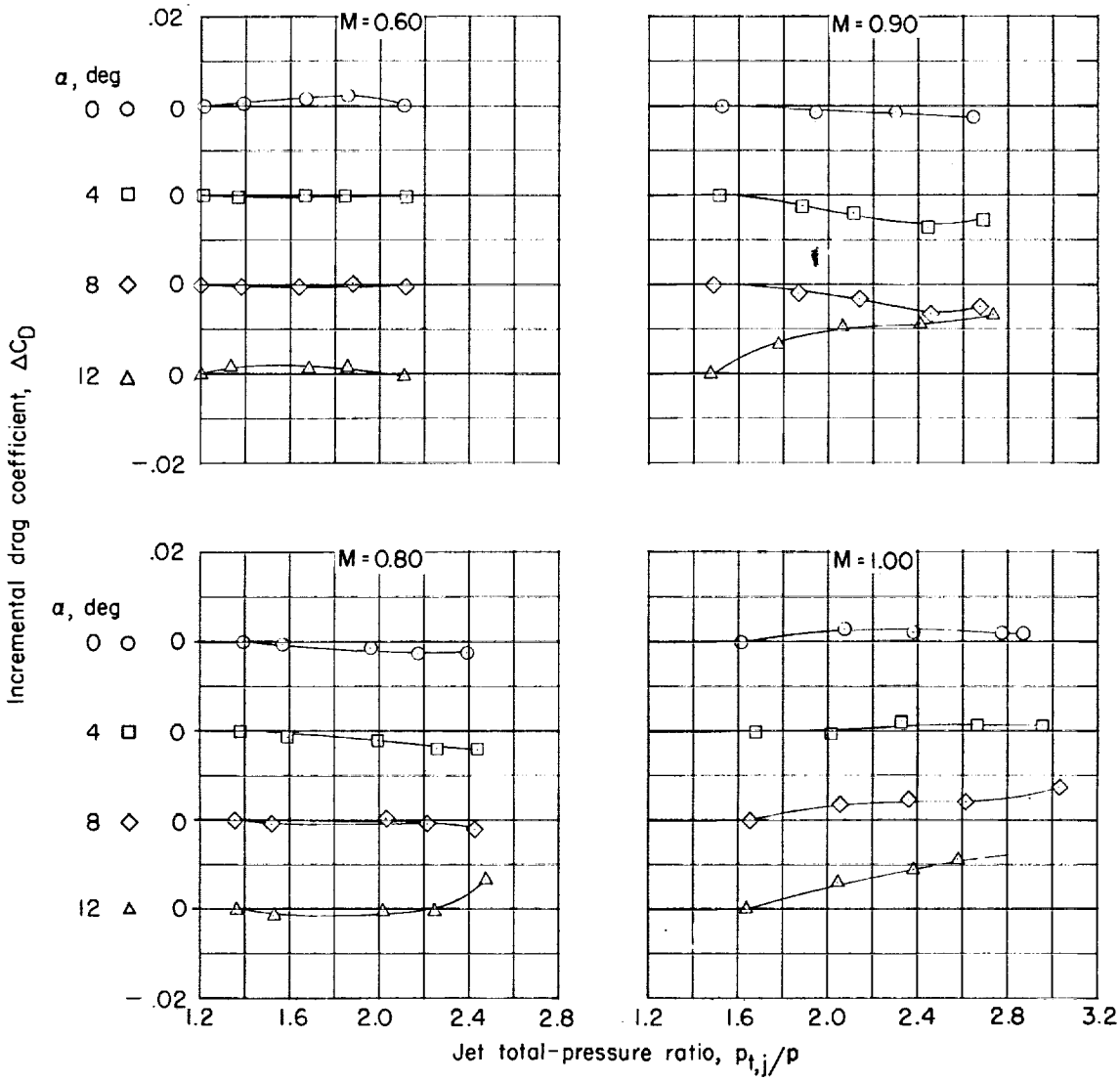

(b) Variation of incremental drag coefficient with jet total-pressure ratio.

Figure 6.- Continued.

[redacted]

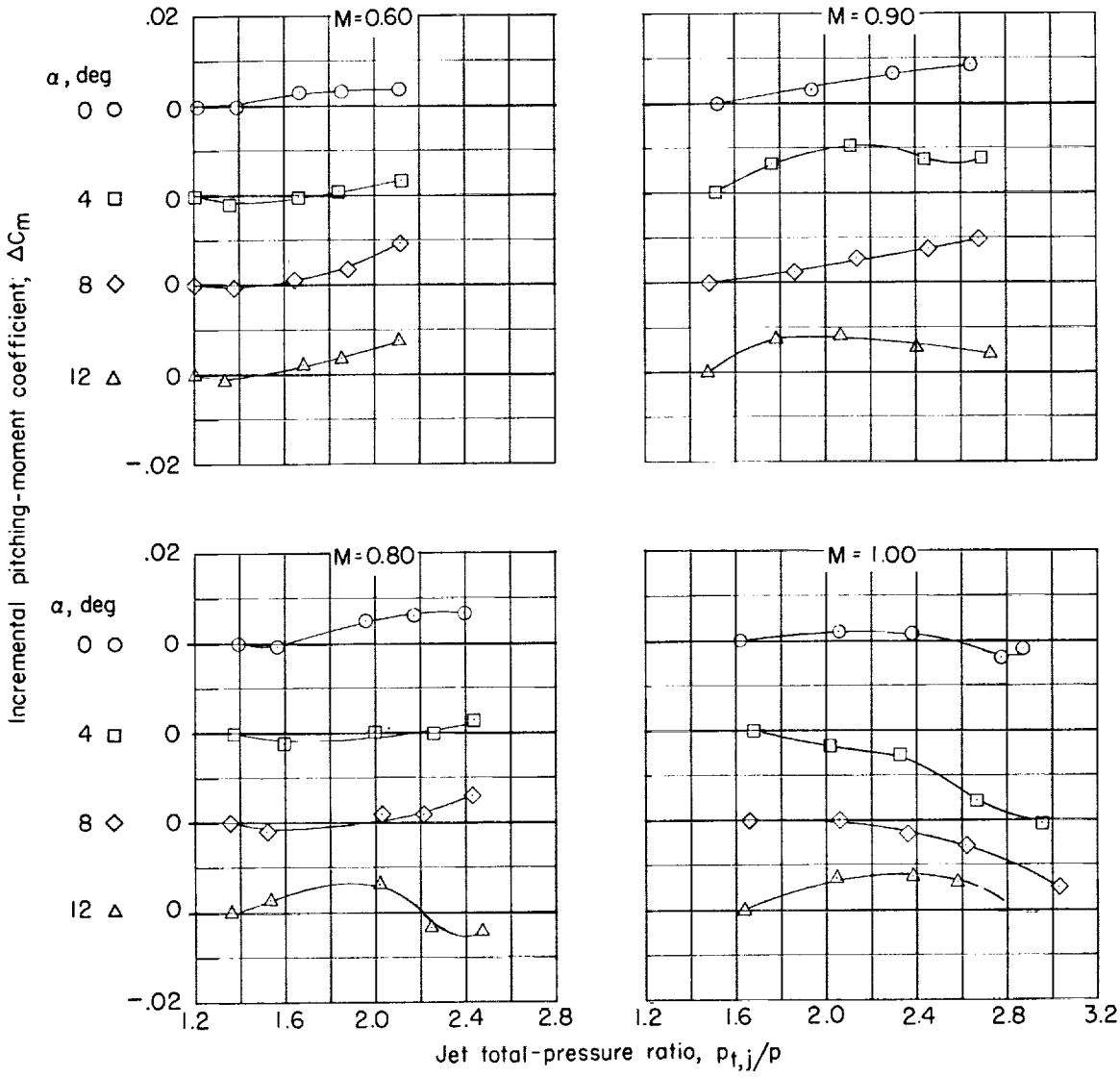

(c) Variation of incremental pitching-moment coefficient with jet total-pressure ratio.

Figure 6.- Concluded.

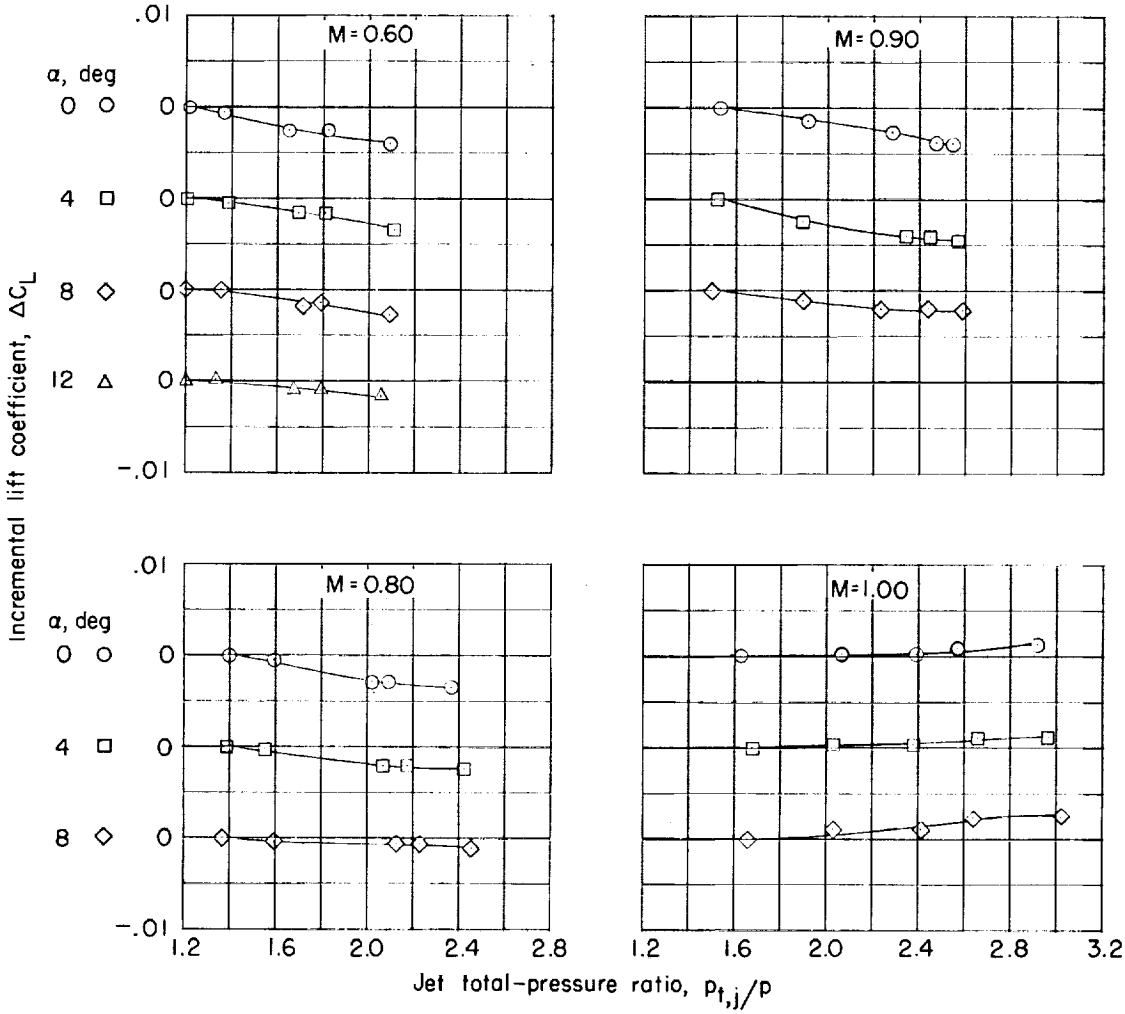

(a) Variation of incremental lift coefficient with jet total-pressure ratio.

Figure 7.- Jet effects on aerodynamic characteristics of model with horizontal-tail incidence set at $i_t = -5^\circ$.

[redacted]

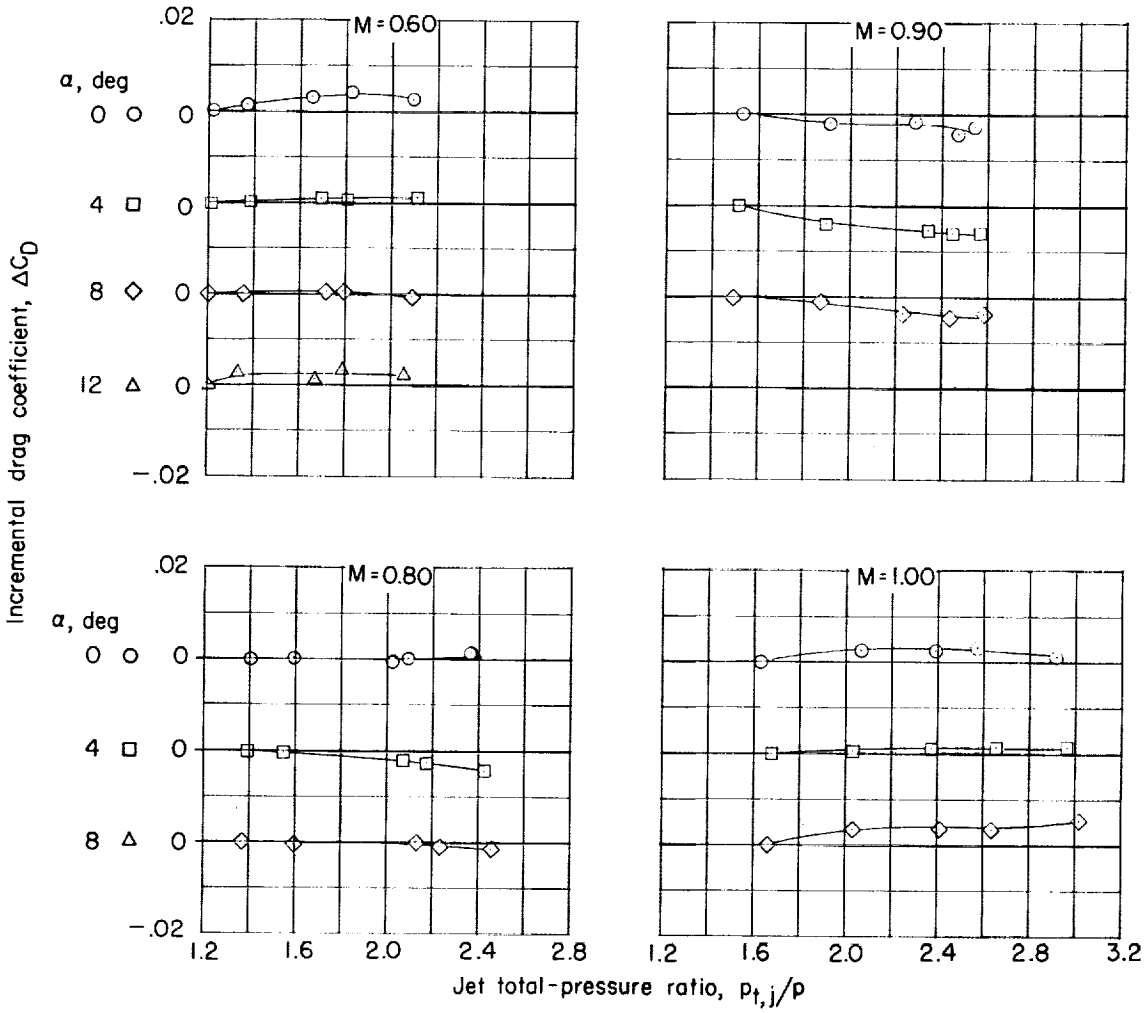

(b) Variation of incremental drag coefficient with jet total-pressure ratio.

Figure 7.- Continued.

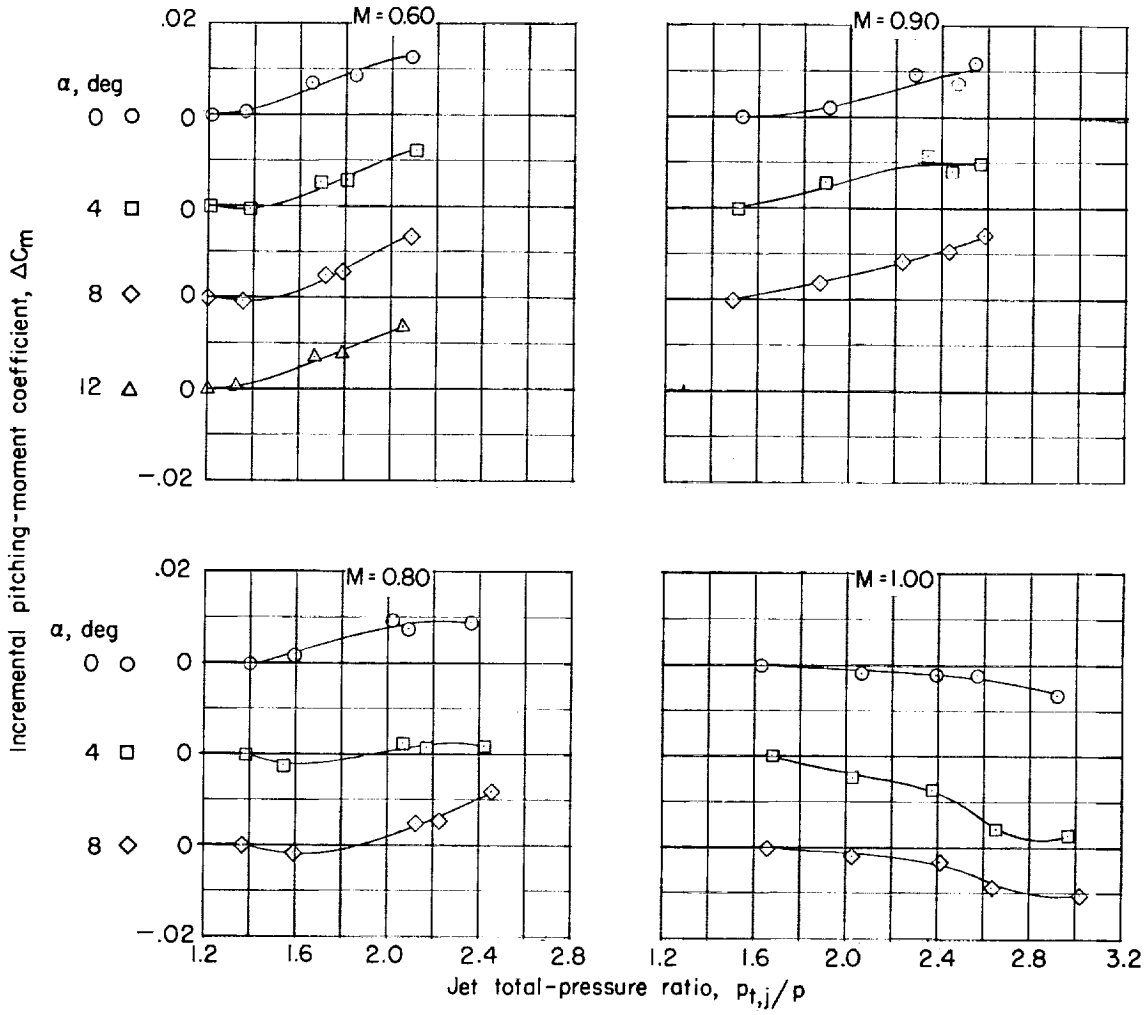

(c) Variation of incremental pitching-moment coefficient with jet total-pressure ratio.

Figure 7.- Concluded.

[redacted]

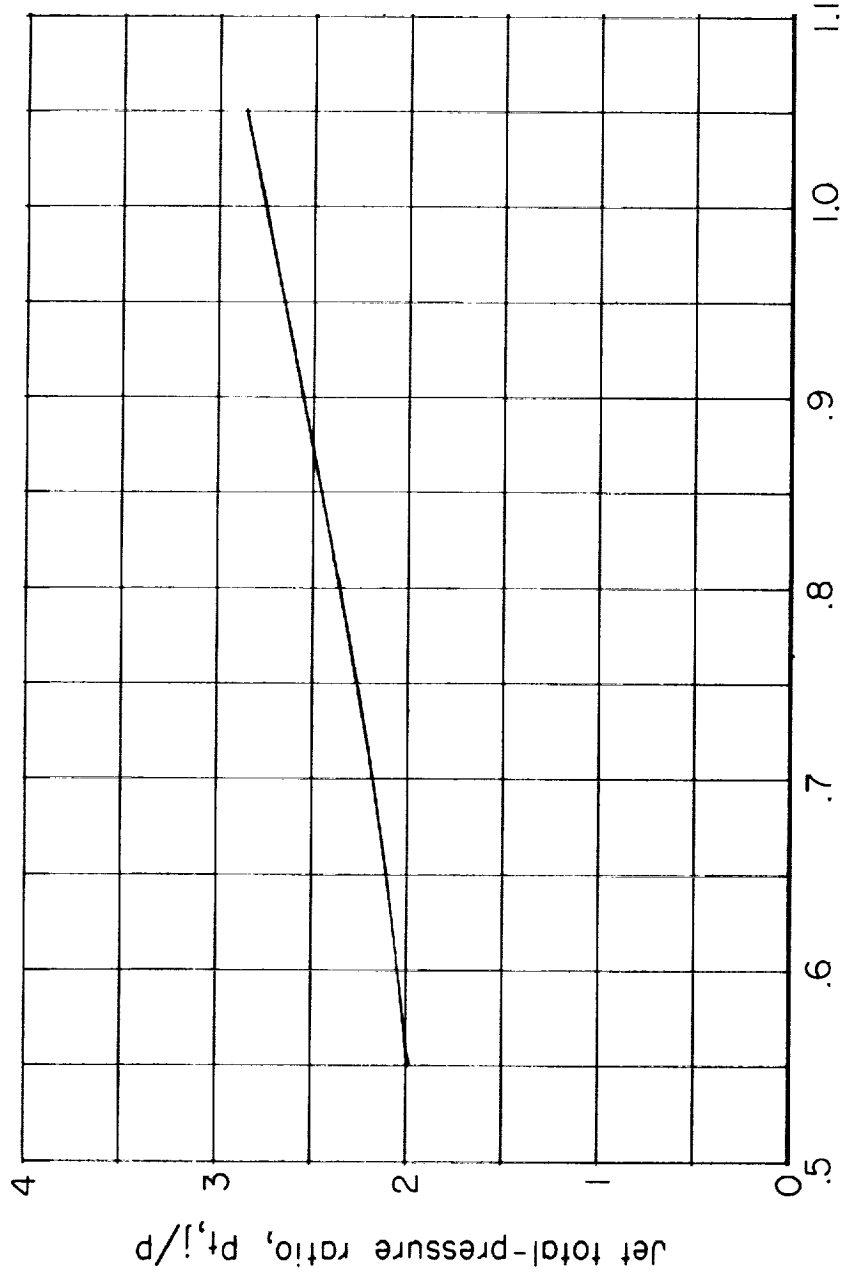

Figure 8.- Assumed schedule of jet total-pressure ratio with Mach number for turbofan engine.

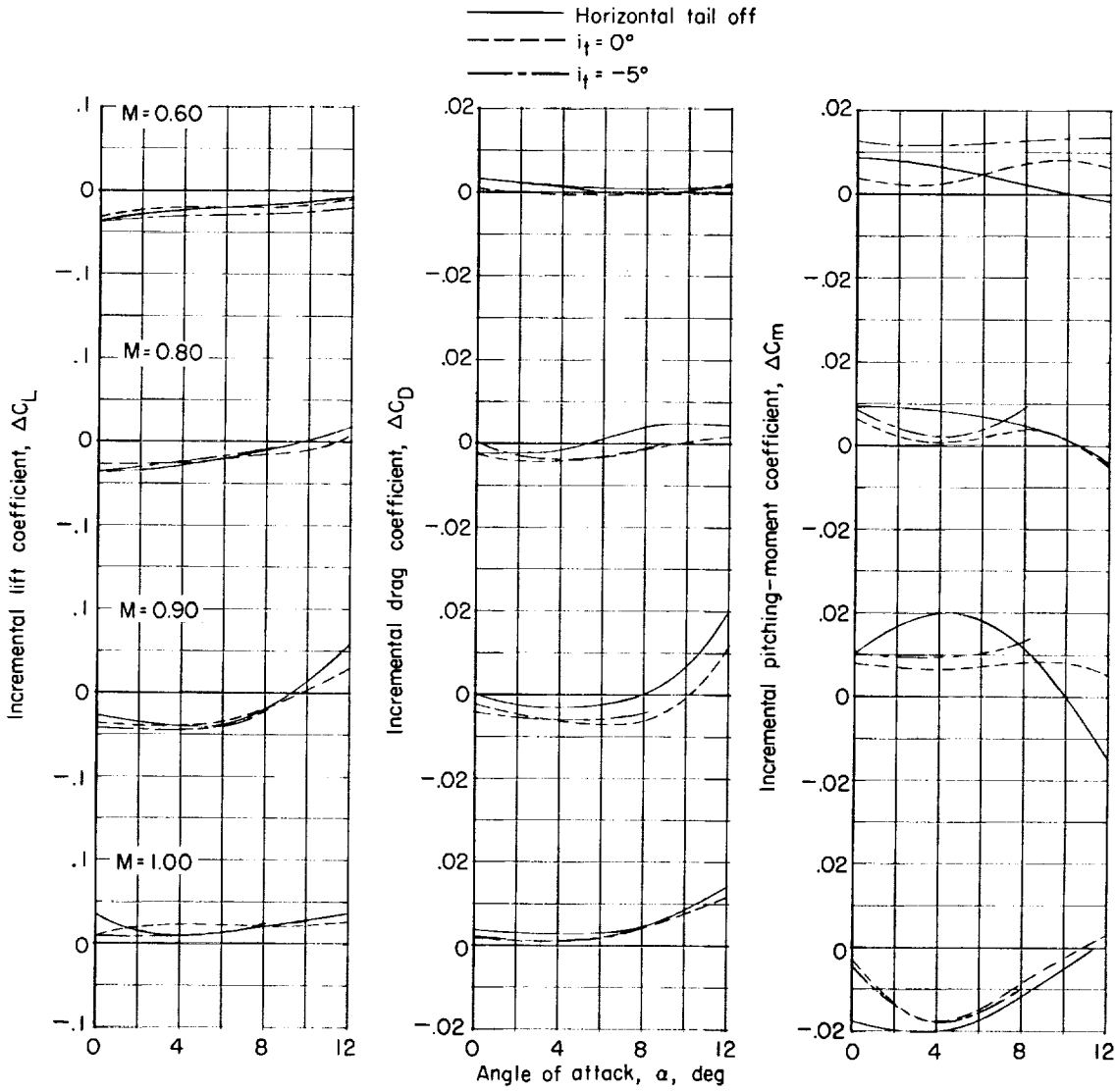

Figure 9.- Jet-induced incremental aerodynamic coefficients for three horizontal-tail configurations.

[redacted]

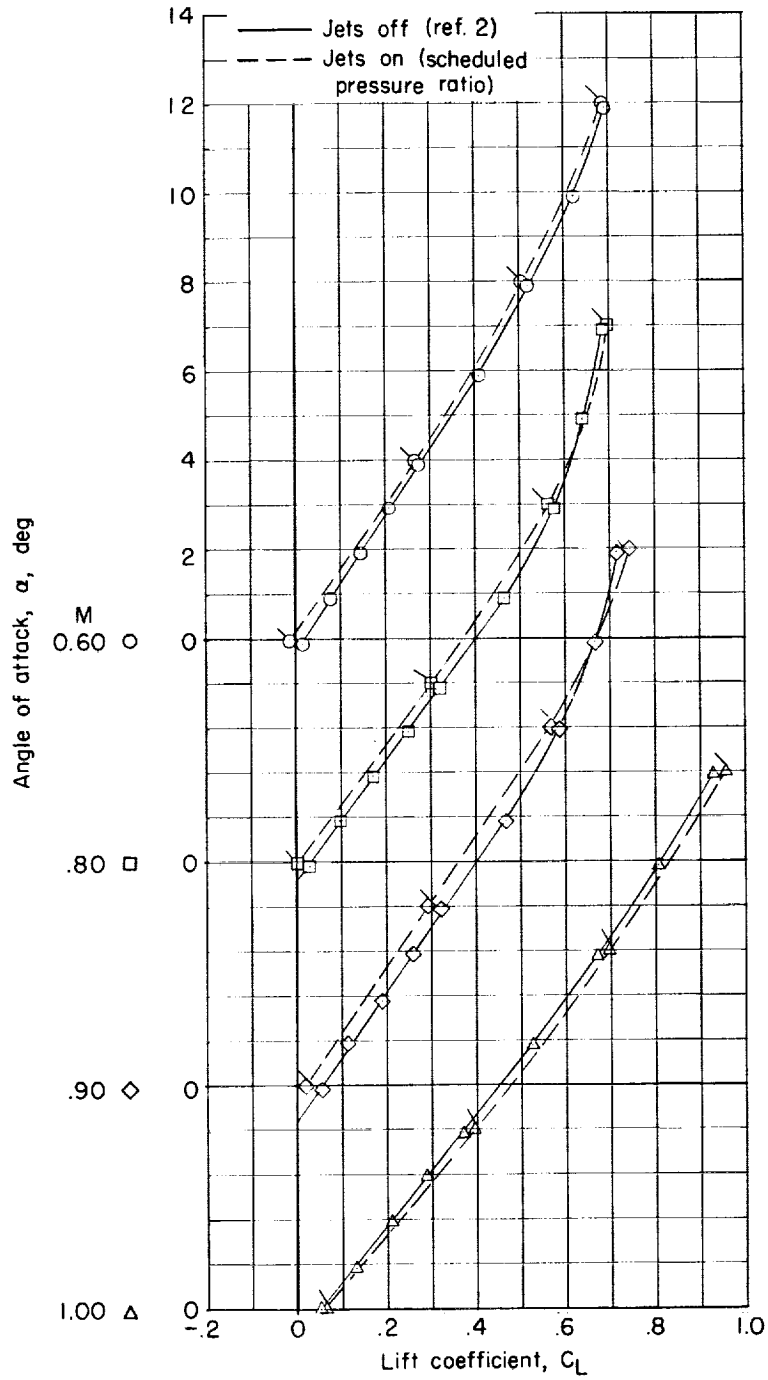

(a) Variation of angle of attack with lift coefficient.

Figure 10.- Aerodynamic coefficients for model with and without jet operation. $i_t = 0^o$. (Flagged symbols denote cross-plotted jet-on data.)

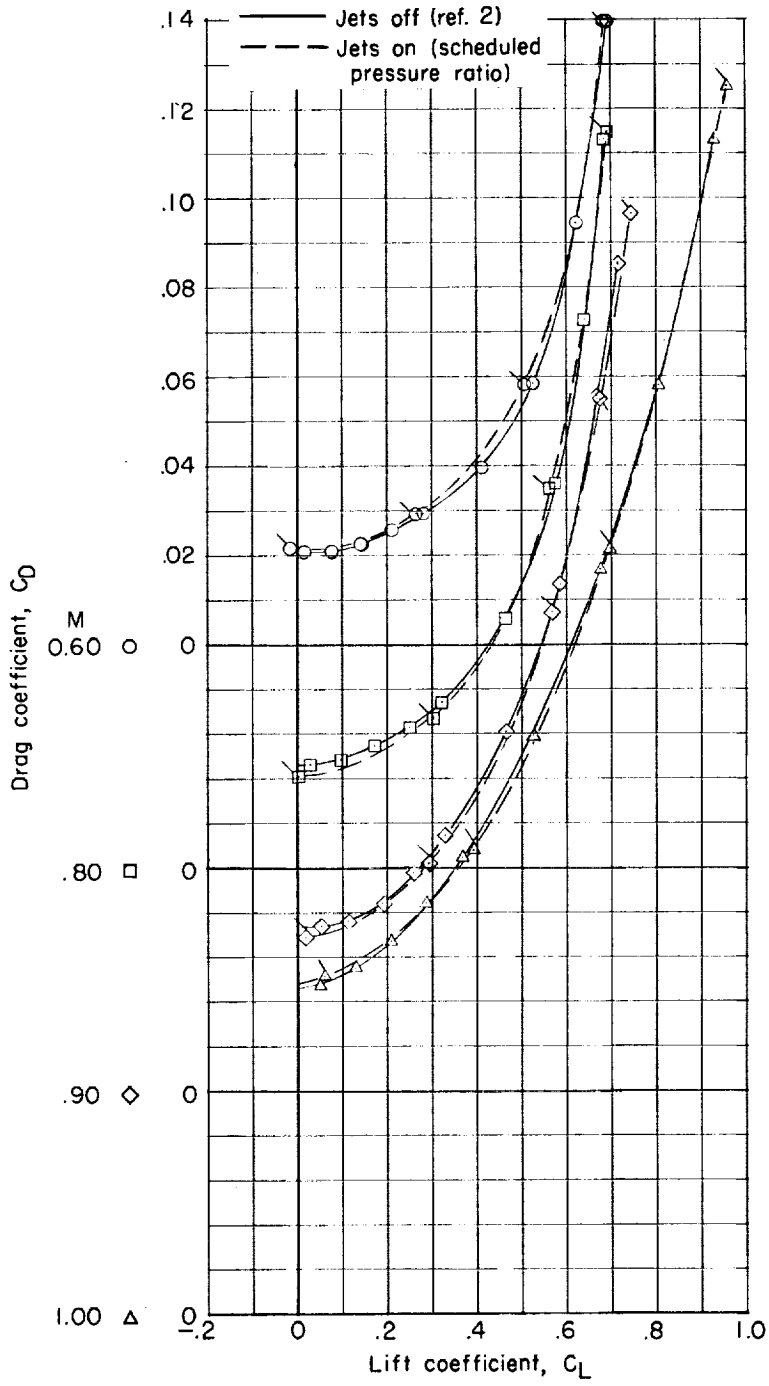

(b) Variation of drag coefficient with lift coefficient.

Figure 10.- Continued.

[redacted]

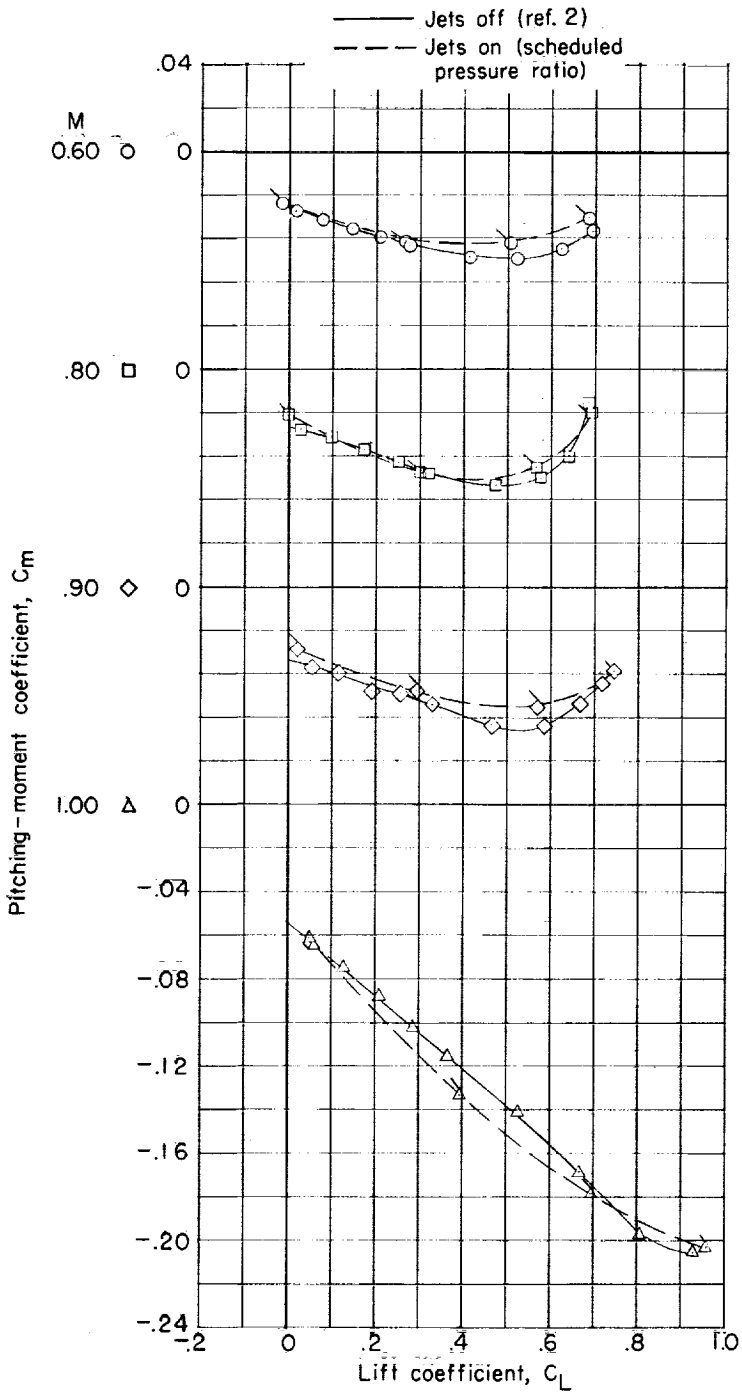

(c) Variation of pitching-moment coefficient with lift coefficient.

Figure 10.- Concluded.

NATIONAL AERONAUTICS AND SPACE ADMINISTRATION

TECHNICAL MEMORANDUM SX-685

for the

U.S. Air Force

JET INTERFERENCE EFFECTS ON A MODEL OF A SINGLE-ENGINE FOUR-JET V/STOL AIRPLANE AT MACH NUMBERS FROM 0.60 TO 1.00*

By James W. Schmeer and Jack F. Runckel

ABSTRACT

The exhaust of the turbofan power plant of the airplane was simulated by inducing tunnel airflow through two large side inlets and injecting hot decomposition products of hydrogen peroxide into the internal flow. Jet effects on the aerodynamic and longitudinal stability coefficients were obtained for the model with horizontal tail removed and at 0° and -5° incidences for Mach numbers from 0.60 to 1.00, angles of attack from 0° to 12°, and jet total-pressure ratios up to 3.1.

*Title, Unclassified.